Proceedings of the Canadian Society for Mechanical Engineering International Congress
32nd Annual Conference of the Computational Fluid Dynamics Society of Canada
Canadian Society of Rheology Symposium
CSME-CFDSC-CSR 2025
May 25–28, 2025, Montréal, Québec, Canada

AI-driven modelling of electrostatic powder coating: Data collection

Haitam Chaouki[1*], Michel Lessard[2], Lucas A. Hof[1], Giuseppe Di Labbio[1]
[1]Department of Mechanical Engineering, École de technologie supérieure (ÉTS), Montréal, QC, Canada
[2]Techologies NeuroBotIA Inc., Québec, QC, Canada
*haitam.chaouki.1@ens.etsmtl.ca, giuseppe.dilabbio@etsmtl.ca, lucas.hof@etsmtl.ca

Abstract — Powder coating has become a popular surface finishing technique in many industries (e.g., home appliances, automotive parts, outdoor products) owing to its durability, corrosion resistance and low environmental impact. While powder recycling systems are often in place to capture non-deposited powder, waste can nonetheless be further reduced by optimizing the uniformity of the applied coating thickness. In this work, an experimental data collection approach is proposed to generate a high-quality database for the training of an AI-driven model of the distribution of electrostatic powder coating on flat surfaces. We propose a novel, scalable, low-cost automated coating thickness measurement system based on a microscopic incision tool, an open hardware CNC machine, a Raspberry Pi and the open source OpenCV image processing library. The system is capable of characterizing the coating thickness distribution of flat plates at a custom spatial resolution (as low as 0.1 mm) in a reasonable time with an accuracy of 2 µm. The proposed system can serve as a quality control and process optimization tool in an industrial workflow.

Keywords: powder coating; coat thickness; coat uniformity

I. INTRODUCTION

Powder coating is widely-used in industry for painting parts given its multiple advantages including its durability, corrosion resistance and eco-friendliness [1]. In this process, an electrostatically-charged dry pigmented powder is applied to a conductive substrate. To set the coat, the coated substrate undergoes a heat treatment during which the powder particles melt and fuse into a cohesive, uniform coating. As opposed to traditional liquid coatings, powder coating has substantially lower volatile organic compound (VOC) emissions, thus less environmental and health-related impacts, while delivering a superior finish quality [1].

Despite its multiple advantages, the performance of the powder coating process is far from being optimal. As identified by Shah et al. [2], the main measures of performance can be grouped into two categories: the first pass transfer efficiency (i.e., the amount of ejected powder actually deposited on the substrate) and the coating quality (e.g., uniformity, finish, adhesion, appearance). Together, the first pass transfer efficiency and the uniformity of the coating are strongly related to the effective use of the powder itself. The optimization of these two attributes is therefore critical to reducing waste and contributing overall to a more sustainable process. However, given the limited research in this area, achieving further performance improvements requires above all effective and reliable modelling of the powder coating process.

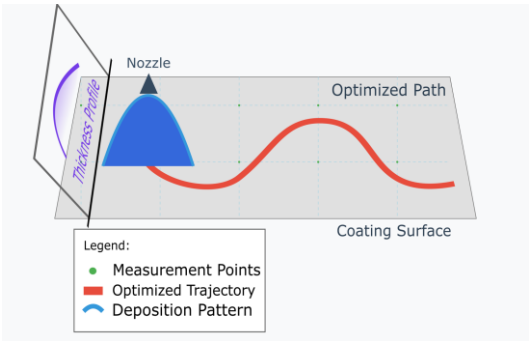

Fig. 1: Schematic of optimal powder coating path to achieve a uniform coating thickness.

Of particular interest in the industrial context, and in this work, is a type of inverse problem, namely, how to best adapt the powder coating path and process parameters to achieve a uniform powder coat over a given object (i.e., in terms of the thickness distribution of the coating); see Fig. 1 for a schematic. The development of such a model presents a significant challenge due to the complex multiphysics nature of the problem and the vast space of input parameters that can influence performance. Moreover, achieving uniform powder coat coverage demands a constant adaptation of the process parameters along the powder coating path to account for geometrical features and electrostatic interactions, further complicating the development of a suitable model.

Fundamentally, the physical problem is governed by a series of differential equations that describe the interactions between the powder particles, the electrostatic field, the substrate and the air [3]. Several studies have used numerical simulations to investigate the effects of physical parameters and operational conditions on performance. For example, Pendar and Páscoa [3] developed a detailed numerical model of the particle trajectories to study, among many aspects, the deposited coating distribution for a rotary bell type sprayer. Particle motion was governed by Eq. (1),

$$m_p \frac{\partial^2 \vec{x}}{\partial t^2} = m_p \frac{\partial \vec{u}_p}{\partial t} = \vec{F}_D + \vec{F}_g + \vec{F}_E + \vec{F}_m \qquad (1)$$

where m_p and u_p represent the mass and velocity of a particle, and the forces (F) from left to right respectively represent drag, buoyancy, the electric force and the added mass force (i.e., inertia of displaced fluid). These forces are coupled to the unsteady compressible Navier-Stokes equation and Poisson's equation for the electric potential. While such an approach provides valuable physical insight, it still requires simplifying assumptions and thus far only considers a stationary sprayer and object (i.e., no prescribed powder coating path). Moreover, the numerical approach is computationally expensive for the purposes of determining coating uniformity and therefore lacks the flexibility to predict coating thickness for different objects and process parameters.

As an alternative to numerical simulation, data-driven phenomenological models can provide adequate predictions of powder coat distribution at a much lower computational cost. This approach often involves modelling the powder coat deposition pattern using compositions of analytical functions, such as Gaussian [4] or β distributions [5], to fit experimental data (e.g., see Fig. 2). Alternatively, experimental thickness distributions can be fitted more closely using splines [6]. In any case, the deposition pattern can then be modulated by the process parameters and deposited along the powder coating path through empirical relationships to generate a prediction of coating uniformity [4,6]. The phenomenological approach has the benefit of inherently capturing the complex physics resulting in the deposition pattern without any particular simplifying assumptions. However, this approach can suffer from over-smoothing, which can suppress details that may in fact be physically important, or over-fitting, which can introduce false features from measurement error. Moreover, the reliability of the deposition patterns and the empirical modulating functions strongly depend on the quantity and quality of available experimental data.

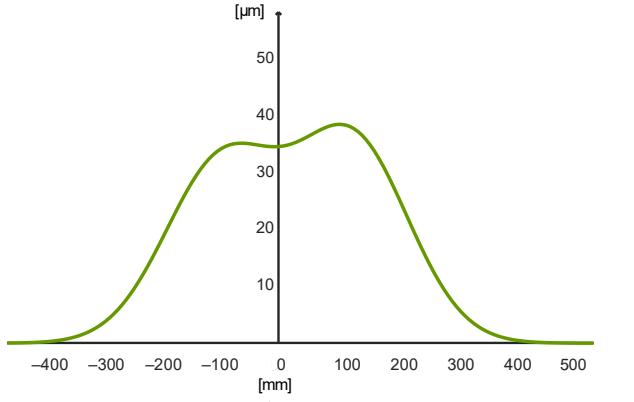

Fig. 2: Example of an analytical paint thickness profile based on the composition of two Gaussian distributions.

With proper training, artificial intelligence (AI) models can produce timely predictions at a reasonable computational cost, overcoming much of the limitations of the numerical and phenomenological approaches. As part of this work, we propose to develop an AI-based model and therefore focus on the first crucial step, namely, data collection. Indeed, the most important and challenging aspect with the development of any AI-based model is the acquisition of a high-quality dataset for training.

As of our main objective is to predict powder coating distributions, we must generate a dataset consisting of accurate coating thickness distribution measurements for a variety of surfaces, powder coating paths and process parameters. We opt for generating the dataset experimentally to avoid the use of simplifying assumptions from numerically-generated data. As a first step, we limit our work to the coating of flat surfaces and develop a system to measure the coating thickness distribution in an accurate, repeatable and scalable manner. The development of this measurement solution is described in detail in section II. The validation of the system and some results are discussed in section III. A conclusion and discussion of future work is provided in section IV.

II. Methodology

Several techniques are available to acquire thickness measurements of coatings, each having their own advantages and disadvantages. A summary of these techniques is provided in Fig. 3, in order of the consecutive improvements made throughout this work. Two commonly used techniques include cross-section analysis and magnetic induction gauges. The former requires cutting samples of the coated part to examine the cross-section under a microscope or with a micrometer to measure the thickness of the coating deposited above the substrate. This technique is however destructive and risks damaging the coating at the locations where the sample is cut, which would invalidate the thickness measurement. Magnetic induction gauges on the other hand are nondestructive and was our initial approach [7]. They measure the distance to a magnetized object through the amplification of an imposed alternating magnetic field. For a powder coated surface, this distance corresponds to the coating thickness. However, other than being limited to magnetizable substrates, these devices

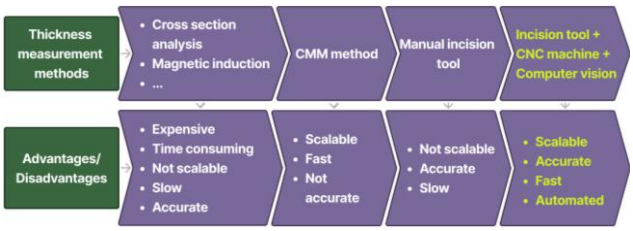

Fig. 3: Schematic overview of techniques to measure powder coating thickness distributions along with their main advantages and disadvantages. The techniques from left to right also represent consecutive improvements in the methodology of our work, as discussed

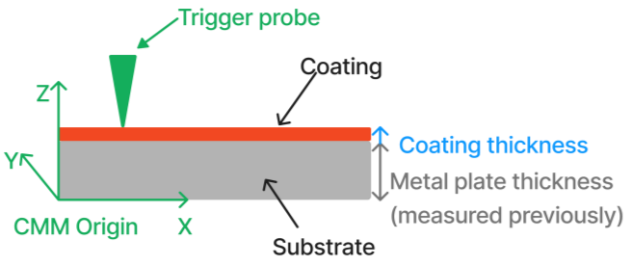

Fig. 4: Measurement of coating thickness using a coordinate-measuring machine (CMM).

often require careful calibration and consist of manual handheld probes, introducing repeatability and scalability issues.

In previous work, we collected a series of flat plates that were powder coated with different process parameters (e.g., nozzle distance, flow rate, travel speed) [7]. We then used a coordinate-measuring machine (CMM) to measure the three-dimensional coordinates of the powder coated flat plates at multiple points [7]. An uncoated portion of the specimen plates was used as a reference *z* coordinate (height) from which the coating thickness was determined at the measurement points (Fig. 4). This technique is also nondestructive and allows, in theory, to map the thickness distribution with high accuracy and spatial resolution in a reasonable time. However, we observed some error as a result of minor curvature of the specimen plates. As a result, the CMM recordings with respect to the uncoated reference included this curvature and biased the measurements. An alternative technique to measure coating thickness that does not suffer from geometrical artifacts is therefore required.

In section II.A, we describe the selected measurement technique that overcomes the difficulties encountered with the CMM. Briefly, as a measure of error for the CMM method, Fig. 5 compares the thickness measurements of a single specimen plate with visible curvature using both the CMM and the new approach detailed in section II.A. In Fig. 5(a), the absolute thickness difference (in µm) is shown for a portion of the plate, where the black circles represent the thickness measurement locations of the CMM and the green stars those of the new approach. Through inspection, we can clearly observe a variation of thickness measurement differences following the

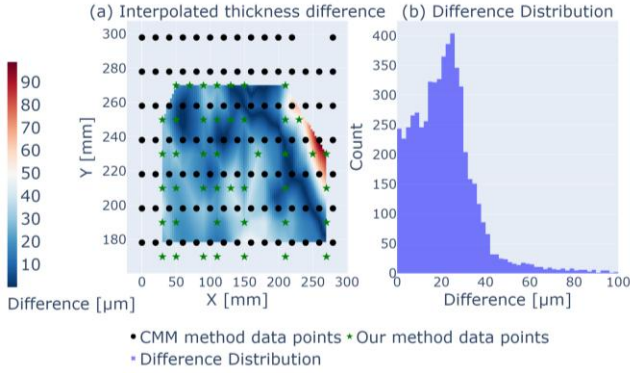

Fig. 5: (a) Distribution of thickness measurement differences between the coordinate-measuring machine (CMM) and the microscopic incision approach over a portion of a specimen plate with visible curvature. (b) Histogram of thickness differences over the plate.

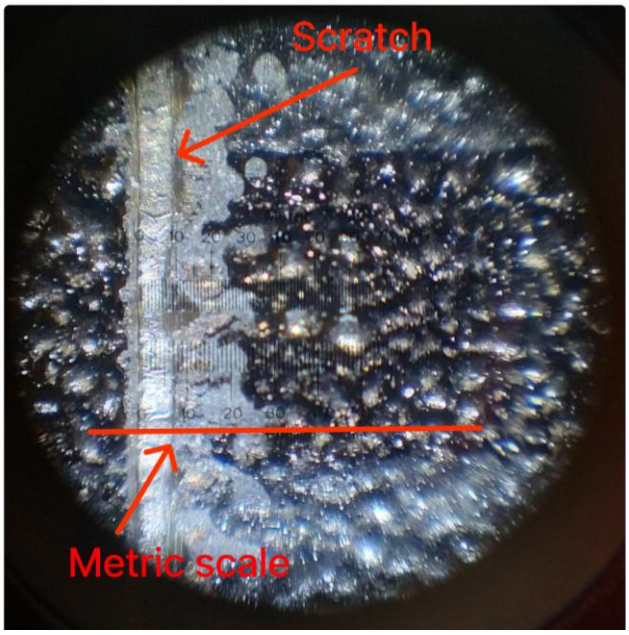

Fig. 6: Microscopic image of an incision made on a specimen plate using the coating thickness measurement tool. The metric scale represents the projected thickness of the incision which is then converted to true thickness (normal to the image plane) based on the known geometry of the incision.

direction of curvature of the plate. In Fig. 5(b), we show a histogram of the differences over the portion of the plate shown in Fig. 5(a), where additional points are sub-sampled using linear interpolation. The average difference is found to be 21 µm with a standard deviation of 14 µm.

A. *Measurement Technique*

In this work, we adopt a technique that measures coating thickness through the analysis of microscopic incisions. The technique uses a handheld device (byko-cut; BYK-Gardner, Wesel, Germany) equipped with a blade, a microscope and a calibrated scale. Incisions are made along the specimen from the coating down to the substrate using an asymmetric V-shaped blade of known geometry. A microscope permits inspection of the V-shaped incision from above, where the coating layer and substrate are visible. In Fig. 6, we show a microscopic photo of an incision made with the tool. By visually comparing the borders of the coating and substrate with the integrated metric scale, we can extract the measurement of the coating thickness. On the left edge of the incision, we observe a thin portion corresponding to the more vertical edge of the V-shaped blade. In the center of the incision, we observe the metallic substrate (marked “scratch” in Fig. 6). On the right edge, we observe a thicker undulating portion corresponding to the more inclined edge of the V-shaped blade which is used to measure the thickness. A calibrated scale (marked in red in Fig. 6) then allows for measurement of the projected thickness (as viewed from above the incision) and conversion to the vertical height of the incision representing the coating thickness. This technique has a rather high accuracy of 2 µm [8] and, although destructive, it allows for repeated measurement of the coating thickness at the incisions as well as the addition of more incisions should more measurement points be required.

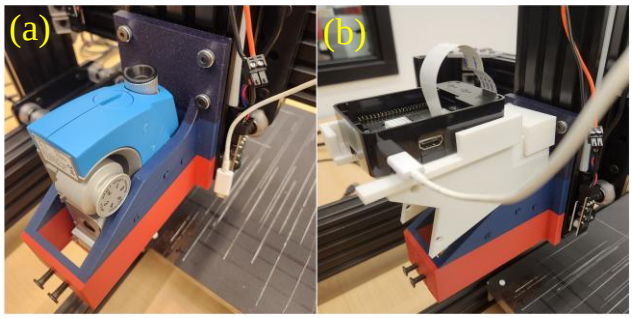

Fig. 7: (a) Mounting assembly for the coating thickness measurement tool on the CNC machine (in scanning mode; the ocular lens is visible). (b) Assembly including the Raspberry Pi and the camera placed over the ocular lens.

We note however that the measurement process using the proposed tool is manual and is therefore rather tedious to use for multiple points and multiple specimens. We must first make incisions with the tool, turn the tool over to use the microscope for thickness measurement (with the naked eye) and then convert this measurement to true thickness using the appropriate factor provided by the manufacturer. In order to solve this scalability challenge, we integrate the cutting tool into a low-cost open hardware computer numerical control (CNC) machine (LEAD CNC Machine 1010; OpenBuilds, Florida, USA) to automate both the incision and measurement processes. The machine's positional accuracy is 0.1 mm in all directions. In order to integrate the cutting tool to the CNC machine, we designed a custom holder fitted to the dimensions of the cutting tool (Fig. 7a) that can accommodate both orientations of the tool.

After several tests, the tool was found to create incisions best without the use of additional force (i.e., the weight of the tool alone is sufficient), and therefore the height of the tool on the CNC machine is adjusted so that the blade rests on the surface of the specimen. We then programmed two modes of use of the CNC machine, namely, an incision mode to make regularly-spaced incisions along the plates and a scanning mode to record the coating thickness (see Fig. 8 for a sample of a series of incisions made on the plate using the incision mode).

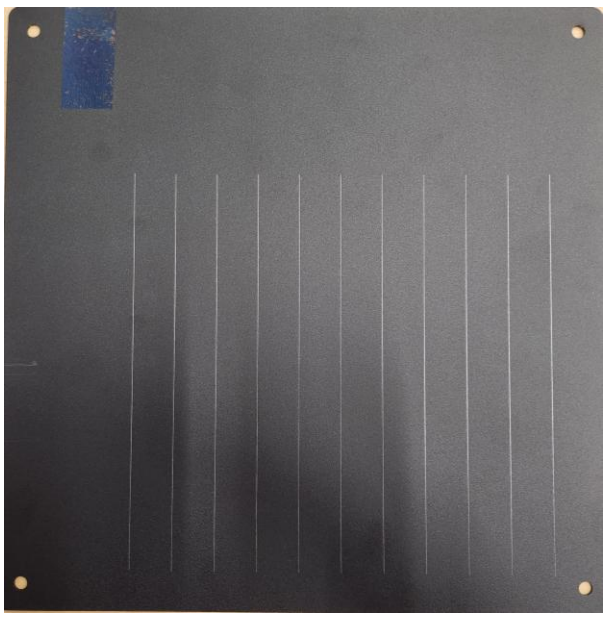

Fig. 8: Sample of a plate with regularly-spaced incisions made using the coating thickness measurement tool automated with a CNC machine.

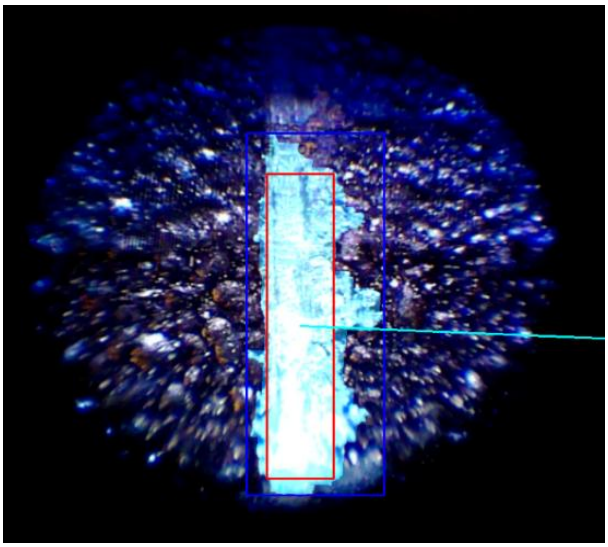

Fig. 9: Example microscopic image of the incision and the identified binary region used to compute the coating thickness.

B. Computer Vision Integration

The microscopic reading of the coating thickness with the proposed tool is also manual, done with the naked eye. In order to automate the reading of the coating thickness, we integrated a Raspberry Pi (Raspberry Pi Foundation, Cambridge, UK) and its associated camera module to the tool holder (see Fig. 7b). The camera is mounted directly above the ocular lens. From the pre-programmed path used to make the incisions, the CNC machine retraces the path and the Raspberry Pi captures the microscopic images at regular intervals. In order to overcome the curvature issue experience with the CMM, we also integrated an autofocus algorithm that acts on the z coordinate in real time to ensure a high-quality image. The algorithm finds the z coordinate that maximizes the Laplacian variance, therefore resulting in a well-focused image [9].

The microscopic images are then analyzed in Python using the OpenCV library; an open-source toolbox for image processing. The recorded images are first converted to grayscale. An edge detection algorithm [10] is then used to extract the incision portion from the image as the largest connected region in the binary mask. The edge detection performs well given the high intensity of the metallic substrate. Using a morphological close operation, the identified region is completely filled (i.e., any gaps are removed) and its boundaries are smoothed (blue region in Fig. 9). To adjust for incision orientation in the image (e.g., as a result of the plate or tool alignment), principal component analysis (PCA) is used to obtain the principal axes of the identified region. The image is rotated to have the incision in a vertical orientation, allowing the horizontal measurement to correspond with the coating thickness. A histogram-based method scans the image row by row and tracks the vertical height of connected white pixels. For each row, the vertical heights are

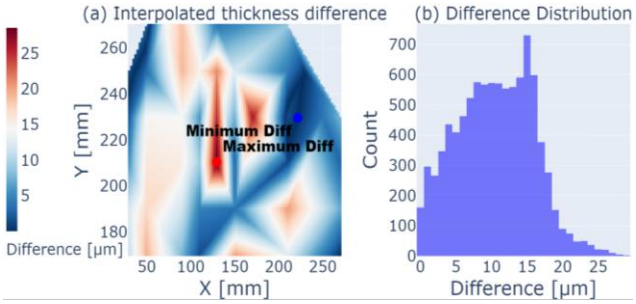

Fig. 10: (a) Distribution of thickness measurement differences between the computer vision algorithm and the naked eye. (b) Histogram of thickness differences over the plate.

adjusted to include connected white pixels and reset to zero if interrupted by black pixels. This information is then used to determine the bounding rectangles that enclose the coating thickness portion of the incision (red and blue rectangles Fig. 9). The coating thickness is then calculated as the average length of the region from the left edge of the inscribed (red) rectangle to the right edge of the circumscribed (blue) rectangle, with a constant value of 10 µm being subtracted representing the horizontal thickness of the incision observed on the metallic substrate. The average thickness is then converted from pixels to micrometers through a predetermined calibration factor.

Notably, the computer vision algorithm can introduce additional error. In order to evaluate this error, we compare measurements made with the presented automated system to those obtained with the naked eye on the integrated microscope at the same points (same images). In Fig. 10(a), we show the distribution of the absolute thickness difference for a sample plate between the two approaches. In Fig. 10(b), we show a histogram of the corresponding differences (as in Fig. 5). The average difference is found to be 10 µm with a standard deviation of 8 µm. Although the difference seems to be rather large, we conclude that it is a result of the difficulty of manually estimating the thickness from the undulations observed on the right edge of the incision in the image. For example, Fig. 11 shows two images post-processed using the algorithm described above at two different measurement points. Images with many undulations on the right edge (Fig. 11a) consistently resulted in higher differences than images with less undulations (Fig. 11b). The average thickness difference between the two approaches is therefore more representative of human error.

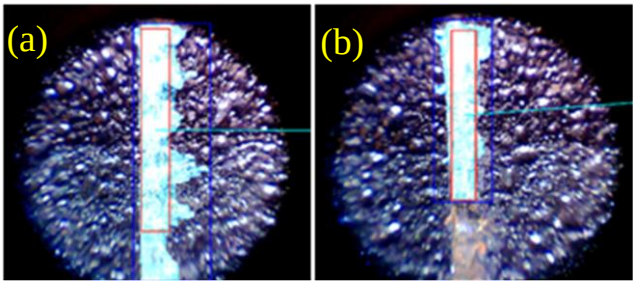

Fig. 11: Images post-processed by the proposed algorithm. (a) A measurement location with many thickness variations. (b) A measurement location with fewer thickness variations.

III. Results & Discussion

In this section, we first aim to validate the presented coating thickness measurement system using a state-of-the-art technique, namely, a laser confocal microscope (section III.A). We then demonstrate the use of the system by fully characterizing and discussing the coating thickness distribution measured for a sample flat plate acquired from previous work [7] (section III.B).

A. *Validation*

In order to validate the coating thickness measurement obtained using the presented automated system, we compare our measurements to those obtained using a laser confocal microscope (LEXT OLS4100; Olympus, Tokyo, Japan) at the same points. The microscope captures the 3D surface map of the incision down to the submicron level (10 nm) [11]. In Fig. 12(a), we show the 3D surface map of the incision obtained using the laser confocal microscope. The red plane indicates a cross-section where the thickness is measured. In Fig. 12(b), the characteristic geometry of the V-shaped incision tool is clearly identified within the cross-section and the coating thickness is evaluated. The average error between the laser confocal microscope and our technique is of the order of 1 µm. This error is based on the average extracted thickness (e.g., Fig. 12b) over all cross-sections of the surface map (e.g., Fig. 12a) for a given sample point. We compare this average thickness to that obtained with our system which includes the same sample point.

B. *Coating Thickness Characterization*

In previous work [7], we collected a series of flat plates that were powder coated manually by an experienced operator for different process parameters such as the number of passes, the current intensity, the sprayer's distance from the plate and more. In order to demonstrate the ability of the presented automated coating thickness measurement system, we select one of these plates and perform a complete measurement process, from incision to scanning to thickness processing. Fig. 13 shows a plate that was painted by executing three consecutive powder

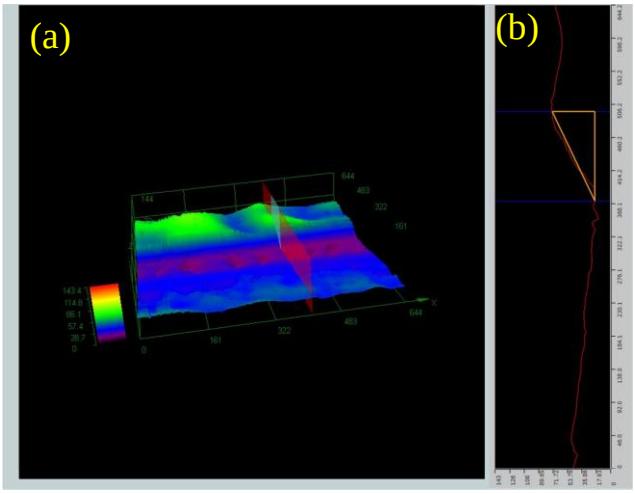

Fig. 12: (a) Three-dimensional surface map acquired by a laser confocal microscope for a sample incision with the red plane showing a sample cross-section. (b) Thickness measurement within the cross-section (red plane).

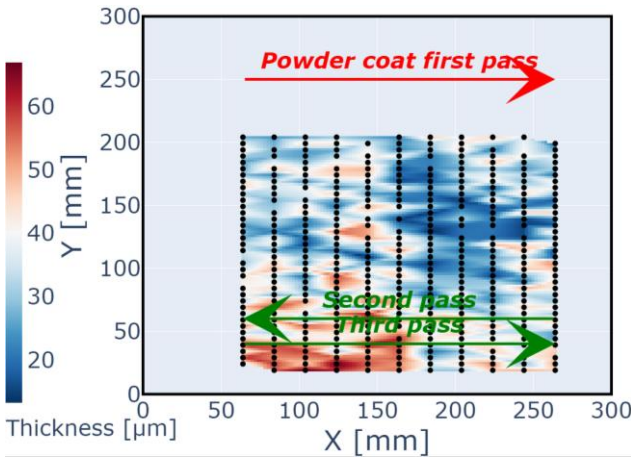

Fig. 13: Interpolated thickness distribution extracted using the presented automated system for a sample plate (plate in Fig. 8). The black rectangle represents the plate dimensions and the black circles the measurement points.

coating passes, one over the top of the plate and two over the bottom of the plate (see Fig. 13). All the passes were done with the following parameters: a perpendicular distance to the plate of 20 cm, a speed of 5 m/s, an electric current of 22 mA and a flow rate of 50%.

In Fig. 13, we also show the resulting coating thickness distribution as measured by the presented automated system. Incisions (vertical lines Fig. 13) were regularly-spaced 20 mm apart and thickness measurements were taken every 5 mm (vertical separation between points in Fig. 13). During data preprocessing, some points are removed as they are identified as outliers. Outliers are identified by calculating the Z-score for each point based on its neighboring points within a radius of 50 mm. Points with a Z-score greater than the threshold of 2 standard deviations are considered outliers and excluded from the dataset. From Fig. 13 we can clearly observe a higher powder coat thickness, around 50 µm on average, towards the bottom of the plate where two passes of powder coating were deposited. Conversely, a lower powder coat thickness is observed, around 20 µm on average, towards the top of the plate where only one pass is deposited.

IV. Conclusion

In this work, we advance the first major step in our objective to develop an AI-based model of powder coating thickness distribution. We focus on the data collection stage where we propose a novel automated coating thickness measurement system. Aside from the microscopic incision thickness measurement tool, the system is based entirely on open software and open hardware. We integrate the measurement tool in a CNC machine and measure coating thickness with a Raspberry Pi (with an associated camera) and OpenCV. The system can characterize coating thickness distributions on flat plates with an accuracy of 2 µm at a spatial resolution down to 1 mm. In future work, we aim to collect and process a series of experimental datasets to begin the development of the AI-driven model. Such a model can further reduce powder waste by achieving a uniform coat. Although we have limited the scope of the system to flat plates, it is scalable and future modifications can permit its use on curved surfaces (i.e., through rotational motions of the incision tool added onto the CNC machine). The proposed system can eventually serve as quality control and process optimization tools in an industrial context.

Acknowledgment

The authors acknowledge support from the Mitacs Accelerate program (IT#31184), Cadence Automation Inc. and Technologies NeuroBotIA Inc.

References

[1] X. Hou et al., “Electrostatic spraying of zinc carbonate hydroxide-infused ethylene-tetrafluoroethylene powders: A thermally-induced, VOC-free antibacterial superhydrophobic coating,” Colloids Surf. A, vol. 705, part 1, p. 135569, Jan. 2025.

[2] U. Shah, C. Zhang, J. Zhu, F. Wang, and R. Martinuzzi, “Validation of a numerical model for the simulation of an electrostatic powder coating process,” Int. J. Multiphase Flow, vol. 33, no. 5, pp. 557–573, May 2019.

[3] M.-R. Pendar and J. C. Páscoa, “Numerical modeling of electrostatic spray painting transfer processes in rotary bell cup for automotive painting,” Int. J. Heat Fluid Flow, vol. 80, p. 108499, Dec. 2019.

[4] D. C. Conner, A. Greenfield, P. N. Atkar, A. A. Rizzi, and H. Choset, “Paint deposition modeling for trajectory planning on automotive surfaces,” IEEE Trans. Automat. Sci. Eng., vol. 2, no. 4, pp. 381–392, Oct. 2005.

[5] W. Xia, S.-R. Yu, and X.-P. Liao, “Paint deposition pattern modeling and estimation for robotic air spray painting on free-form surface using the curvature circle method,” Ind. Rob., vol. 37, no. 2, pp. 202–213, Mar. 2010.

[6] D. Gleeson et al., “Generating optimized trajectories for robotic spray painting,” IEEE Trans. Automat. Sci. Eng., vol. 19, no. 3, pp. 1380–1391, July 2022.

[7] L. Rayeh, G. Di Labbio, and L. A. Hof, “Electrostatic powder coating simulation for an automated robotic paint unit,” Prog. Can. Mech. Eng., vol. 6, p. 335, May 2023.

[8] “Destructive Film Thickness Gauge”, accessed Feb. 10, 2025, https://www.byk-instruments.com/en/Physical-Properties/Coating-Thickness-Gauges/Dry-Film-Thickness%2C-destructive/Destructive-Film-Thickness-Gauge/c/p-15722?variant=3430

[9] R. Bansal, G. Raj and T. Choudhury, "Blur image detection using Laplacian operator and Open-CV," 2016 International Conference System Modeling & Advancement in Research Trends (SMART), Moradabad, India, pp. 63-67, 2016.

[10] S. Suzuki and K. Abe, “Topological structural analysis of digitized binary images by border following,” Comput. Vis. Graphics Image Process., vol. 30, no. 1, pp. 32–46, Apr. 1985.

[11] “OLS4100 Industrial Laser Confocal Microscopes - Olympus 3D Laser Measuring Solution”, accessed Feb. 10, 2025, https://industrial.evidentscientific.com.cn/en/metrology/ols4100/